BILINGUAL PUBLISHING GROUP
Pioneer of Global Academics Since 1984

Journal of Mechanical Materials and Mechanics Research
https://journals.bilpubgroup.com/index.php/jmmmr

ARTICLE

Estimation and Analysis of Structural Responses of Asphalt Pavement Using Interlayer Contact Bonding Model

***Xuntao Wang*[1*], *Hu Wang*[2]**

[1] *Xi'an Shiyou University, Xi'an, Shaanxi, 710065, China*
[2] *Chang'an University, Xi'an, Shaanxi, 710064, China*

ABSTRACT

The interlayer contact condition of asphalt pavement has a significant impact on stress transfer and energy dissipation with adjacent layers, so a model considering the bonding condition of adjacent layers is introduced for evaluating the structural response of asphalt pavement. The pavement structure, the material characterization with temperature, the interlayer contact bonding model, the types of bond failure, and the prediction method of pavement life are described in detail. Results show that the transversely tensile strains at the top of asphalt pavement under the condition of high temperature were easy to cause the top-down cracking outside the edge of the dual tire. The bonding failure has a significant influence on strains at the bottom of the surface course with the condition of high temperature, especially, the longitudinally tensile strains would increase obviously as the disengaging area between the surface course of asphalt pavement and the base layer increases. Finally, it is proved that the surface course is vulnerable to form deformations and cause damage under the combined action of low speed and high temperature

Keywords: Asphalt pavement; Interlayer contact; Bonding condition; Structural response; Strain

1. Introduction

Asphalt pavement is widely used in pavement design and actual engineering due to the effectiveness of distributing and transferring the vehicle load to the subgrade layers. Up to now the evaluation model of the structural response of asphalt pavement is still a crucial part of pavement design and performance prediction. Asphalt pavement is routinely described as a multi-layer composite structure, and the structur-

*CORRESPONDING AUTHOR:
Xuntao Wang, Xi'an Shiyou University, Xi'an, Shaanxi, 710065, China; Email: wxt5288@126.com

ARTICLE INFO
Received: 26 November 2022 | Revised: 30 December 2022 | Accepted: 13 January 2023 | Published Online: 16 February 2023
DOI: https://doi.org/10.30564/jmmmr.v6i1.5288

CITATION
Wang, X.T., Wang, H., 2023. Estimation and Analysis of Structural Responses of Asphalt Pavement Using Interlayer Contact Bonding Model. Journal of Mechanical Materials and Mechanics Research. 6(1): 1-15. DOI: https://doi.org/10.30564/jmmmr.v6i1.5288

al responses of this system are significantly affected by the interlayer condition between adjacent layers [1]. A good interlayer condition between adjacent layers will increase the strength at the contact interface and make different layers of pavement form a monolithic structure to resist the action from the environment and traffic. In contrast, the shear strength between pavement layers will be reduced, and it will be easy to cause pavement distresses and shorten the service life of the asphalt pavement.

There are two common assumptions of interlayer condition between adjacent layers in some previous research [2-4], one is full-bond condition and the other is no-bond condition. However, this is an impractical assumption and an extreme condition to the real pavement structure. BISAR software was usually used to simulate the pavement structure and compute the response of asphalt pavement [5,6]. The model in BISAR generally uses some possible values of the sliding coefficient to simulate the interface condition. Nevertheless, it is difficult to obtain the real value of the sliding coefficient and can't simulate the actual interlayer contact condition of adjacent layers. Some researchers [1,7,8] held the interlayer condition of pavement structure lies in someplace between the bonded condition and the unbonded condition. In this research, the contact element and target element are applied to simulate the function of bonding material between adjacent layers, and this is different from the finite element calculation of previous studies. Otherwise, the model used in this paper is the interlayer contact bonding model, and it will be explained and illustrated in the following text.

Previous research has shown that the interlayer bonding condition plays an important role in accurately calculating and predicting the responses of asphalt pavement [9-11]. So this paper will investigate the structural responses of asphalt pavement with the interlayer contact bonding model and analyze the pavement performance. The Modified Havriliak—Negami model is utilized to describe material characteristics of asphalt mixtures at different frequencies and temperatures, and construct the dynamic modulus master curve of asphalt mixtures according to the datum from the citation. The detailed calculations for the structural responses of the typical asphalt pavement were executed under vehicle load and different temperatures.

2. Methodology

2.1 Pavement structure and vehicle loading

The road structure is comprised of four different layers from top to bottom [12], which includes the asphalt concrete layer, semi-rigid base, subbase, and subgrade. Meanwhile, the asphalt concrete layer (the surface course) is divided into three sublayers, the upper layer (ACUL for short), middle layer (ACML for short) and lower layer (ACLL for short). The pavement structure is shown in **Figure 1**, which is symmetric along the Y axis. For the purpose of minimizing the effect of boundary condition and mesh size on finite element calculation in ANSYS, the final structure size of asphalt pavement is 305 cm in width and 720 cm in length, and this is gotten by a large number of numerical tests and previous experiences. The structural responses at different locations of asphalt pavement are monitored by using the three points shown in **Figure 1**, and these responses are the displacement of point A, which locates at the surface of ACUL along the Y direction (U_{YA} for short), the strains of point B, which locates at the bottom of ACLL along the X direction and the Z direction (ε_{XB} and ε_{ZB} for short), and the strain of point C, which locates at the top of subgrade along the Y direction (ε_{YC} for short), respectively. In this study, these responses will be applied to predict the behaviors of asphalt pavement and analyse the performance of the pavement structure [13,14].

The mesh size near the loading area is relatively fine, and the meshing is 5 cm along X direction and 4.5 cm along Z direction, respectively. The mesh size in other areas is relatively coarser, and the meshing is 10 cm along X direction and 9 cm along Z direction, respectively. The finite element model of the pavement structure is shown in **Figure 2**. There is a vehicle load with a single tire, which is applied on the surface of ACUL, and the tire load is 0.7 MPa. It

is assumed that the loading footprint is a rectangle, which is 20 cm long and 18 cm wide [15-17]. In addition, considering the action of rolling friction between the tire and ACUL in the horizontal, the force of rolling friction f between them is determined by Equation (1):

$$f = \mu P \tag{1}$$

in which μ is the coefficient of rolling friction, and it equals 0.012 in this study. P represents pressure.

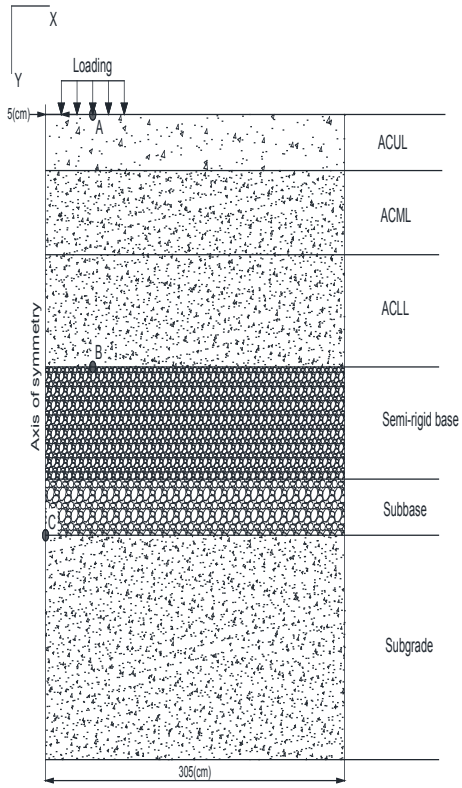

Figure 1. Mesh of pavement structure and monitoring points (Not to scale).

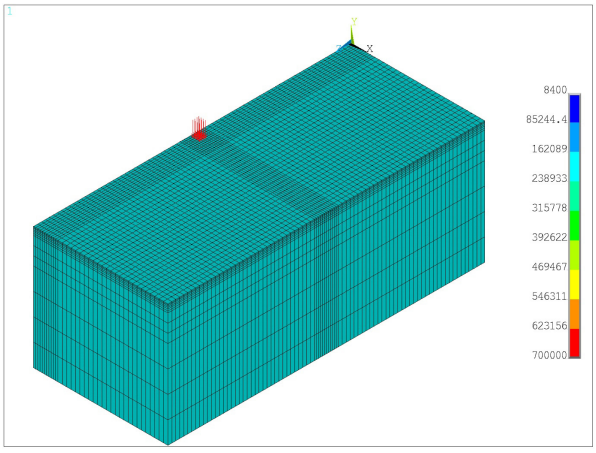

Figure 2. The finite element model of the pavement structure.

2.2 Material characterization

Asphalt mixture has the characteristics of viscoelastic material, and its responses are mainly affected by two factors. One is environment temperature, and the other is loading frequency. Therefore, the dynamic modulus master curve can be utilized for the characterization of the behavior of viscoelastic material, and also used to reflect the performance and behaviors of asphalt concrete. Generally, dynamic modulus $|E^*|$ and phase angle φ are measured by test [18], and they satisfy the following equations:

$$\begin{cases} E^* = E' + iE'' \\ |E^*| = \sqrt{(E')^2 + (E'')^2} \\ E' = |E^*|\cos\varphi,\ E'' = |E^*|\sin\varphi \\ \tan\varphi = E''/E' \end{cases} \tag{2}$$

where $i = \sqrt{-1}$ = unit imaginary number. E' is storage modulus, and E'' is loss modulus. In this research, the dynamic modulus master curve of the asphalt mixtures is constructed by the Modified Havriliak–Negami (MHN) model [18,19], where the loading frequency and environment temperature are taken into account, and it has the following form:

$$E^*(\omega) = E_0 + \frac{E_\infty - E_0}{\left[1 + \left(\frac{\omega_0}{i\omega}\right)^\alpha\right]^\beta} \tag{3}$$

where ω means angular frequency. E_0 is complex modulus when ω approaches 0, and E_∞ is complex modulus when ω approaches ∞. ω_0 is related to the time-temperature shifting and controls the horizontal position of the master curve. α and β are all parameters of the MHN model. Based on the time-temperature superposition principle (TTSP), the influences of loading frequency and environment temperature can be merged into one variable, and this is reduced frequency ω_r, which is defined as follows:

$$\omega_r = \omega \times \alpha_T \tag{4}$$

where α_T is time-temperature shift factor. The Williams-Landel-Ferry (WLF) equation is the most common model for the time-temperature shift factor of asphalt concrete, where α_T is a function of temperature T, as follows:

$$\alpha_T = \frac{-C_1(T-T_0)}{C_2+(T-T_0)} \tag{5}$$

C_1 and C_2 are two parameters of the equation. T_0 denotes reference temperature. Then the dynamic modulus of material at different temperatures can be obtained from the equation of the master curve by replacing the physical frequency with the reduced frequency at the reference temperature, as follows:

$$E^*(\omega,T)=E^*(\omega_r,T_0) \tag{6}$$

The MHN model coefficients of three kinds of asphalt mixture used in this paper are presented in **Table 1**, and the datum is from the reference [18]. It chooses 25 °C as the reference temperature, and the reduced frequency is 5 Hz, which is the typical frequency induced by a truck travelling at 80 km/h on asphalt pavement [11,20].

Compared with the normal temperature, asphalt pavement is more prone to form deformation and damage with the high temperature. Because the material properties of asphalt concrete are related to the environmental temperature. Therefore, the responses of the asphalt pavement structure will be considered at the normal and high temperatures in this research respectively. To obtain the dynamic modulus of each sublayer of asphalt concrete layer at different temperatures, the temperature of each sublayer must be determined first. It is assumed that the temperature of each sublayer of the asphalt concrete layer is changing with the depth of the pavement, and then the empirical formula (7) is used to estimate the temperature of three sublayers of asphalt concrete layer at the high temperature [6]:

$$T = 54.32 + 0.78T_{air} - 0.0025\mathrm{Lat}^2 - 15.14\lg(H+25) \tag{7}$$

where T means the estimated value of the temperature of each structural layer (°C). T_{air} denotes the mean value of maximum temperature within one week (°C). Lat represents the latitude of the area where the asphalt pavement is located (°), and H means the depth of the sublayer from the top of the surface course (mm). Take Xi'an city (in China) as an example, then $T_{air}=36$ (°C, in Summer), $\mathrm{Lat}=34$ (°). Now the temperature of the three sublayers of the asphalt concrete layer in Summer can be determined according to Equation (7). In **Table 2**, the related material parameters of asphalt pavement structure are listed, and the responses of the pavement will be computed at the normal temperature and the high temperature for analyzing the performance of the asphalt pavement.

2.3 Bonding model between adjacent layers

The bonding condition between adjacent layers of asphalt pavement has an obvious influence on the stress transmission and energy dissipation of pavement structure [21], and also affects the prediction of structural responses of asphalt pavement. Therefore, the interlayer condition between adjacent layers is considered to be the interlayer contact bonding condition (ICB condition) in the study, and the interlayer contact bonding model (ICB model) is introduced to simulate realistic interface behavior [17]. The ICB model can be illustrated in **Figure 3**, where the bottom of ACUL cover with contact elements, and the top of ACML is covered with target elements. Spring elements are used to connect the contact elements and the target elements by the corresponding nodes. Meanwhile, other contact interfaces of adjacent layers are all connected in the same way, and then there are totally five contact interfaces as shown in **Figure 3**.

In the ICB condition, the stress is calculated by the contact algorithm according to the length of compression or tension of springs at the corresponding nodes [22]. Each spring has three characteristic parameters, and these parameters are usually created automatically with a contact algorithm on the basis of the mesh size of the finite element and the relevant parameters of material characteristics. But sometimes these parameters need to be adjusted to get a better and convergent solution.

Table 1. The model coefficients of asphalt mixture.

Type	E_0 (MPa)	E_∞ (MPa)	α	β	ω_0	C_1	C_2
SMA13	51.1	26317	0.266	1.693	657.1	21.7	183.5
Sup20	104.8	32128	0.257	1.733	407.9	15.3	139.0
Sup25	35.9	24558	0.296	1.504	612.0	23.1	191.4

Table 2. Material parameters of asphalt pavement structure.

Layer	Normal temperature (°C)	High temperature (°C)	Modulus (MPa)	Poisson's ratio	Density (kg/m^3)	Thickness (cm)
ACUL(SMA13)	20	54(*H*=20)	Determined from master curve	0.30	2350	4
ACML(Sup20)	20	49(*H*=70)		0.30	2360	6
ACLL(Sup25)	20	46(*H*=140)		0.30	2370	8
Base	-	-	1200	0.25	2300	40
Subbase	-	-	300	0.35	1932	20
Subgrade	-	-	50	0.40	1926	200

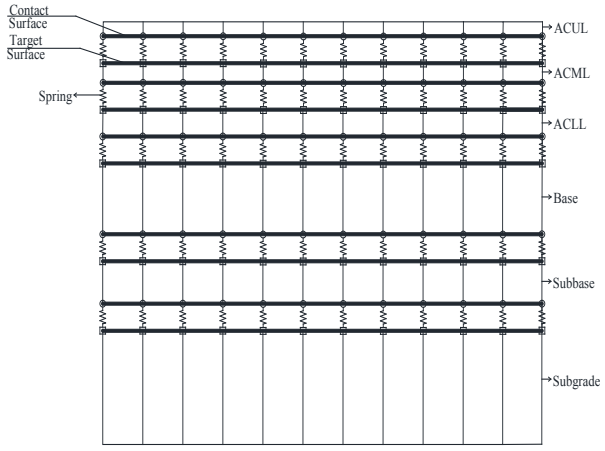

Figure 3. Schematic of ICB model.

In the ICB model, the augmented Lagrangian method is used to calculate the contact stress in the normal and tangential direction [22], and the tangential stress at the contact interface satisfies the following relation:

$$\tau_{\lim} = \mu P + b \tag{8}$$

$$|\tau| \le \tau_{\lim} \tag{9}$$

where $\tau_{\lim}$ is ultimate stress in a tangential direction, μ denotes the coefficient of sliding friction, P means the normal compressive stress, b represents the adhesion stress of the contact interface; τ is the shear stress in the tangential direction. In Equation (8), if μ equals zero or P equals zero, b is not zero, adjacent layers may keep sticking state and no sliding. If b equals zero, this means that there is no bond stress between adjacent layers or adjacent layers appear bond failure. If inequality (9) holds, namely $|\tau|$ is less than or equals $\tau_{\lim}$, the adjacent layers still keep sticking state. Otherwise, there will be relative sliding between adjacent layers. Five contact interfaces are created in **Figure 3**, where the adhesion stress is 0.45 MPa in the three upper interfaces [23], and the adhesion stress is all 0.01 MPa in the other two lower interfaces.

Due to constructional deficiency or the chronic and repeated action of environment and traffic, bond failure between adjacent layers may occur during the service life of asphalt pavement and form the disengaging area. The ICB model can simulate the variation of interlayer bonding conditions by adjusting the value of b. If the bond failure occurs somewhere between the adjacent layers, b in Equation (8) is 0 in disengaging area and unchanged in other areas. In order to facilitate the simulation and calculation, there are five types of disengaging areas to imitate the phenomenon of bond failure,

and they were shown in **Figure 4**. The dashed box in **Figure 4** all means the load region on the surface of ACUL. The shaded area denotes the disengaging area under the load region, and it means that the phenomenon of the local bond failure occurs at the contact interface. In type "T0", the disengaging area is 0, and this means that the adjacent layers keep good bonding condition and no disengaging area appear between the two adjacent layers. In type "T1", the disengaging area is 10×9 cm^2 under the load region, and this denotes that the disengaging area between two adjacent layers is 10 cm in length and 9 cm in width. In type "T2", the disengaging area is 20×18 cm^2 under the load region, and it is the same size as the load region on the surface of ACUL. Besides, types "T3" and "T4" have a similar meaning to the type "T2", but the size of the disengaging area is bigger than the size of the type "T2".

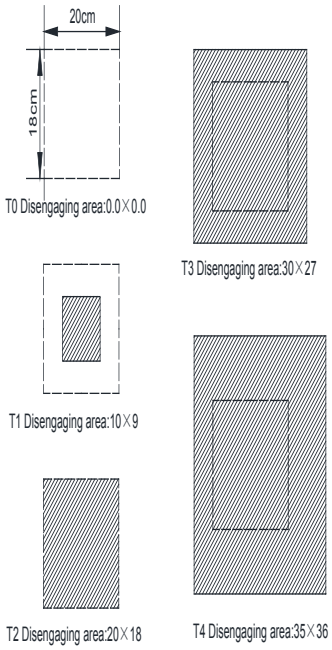

Figure 4. Type of disengaging area under loading area (Not to scale, Unit: cm^2).

2.4 Pavement life prediction method

For the purpose of discussing the effect of interlayer conditions of adjacent layers and temperature on the responses of the asphalt pavement structure, four cases are considered as follows:

Case 1: the interlayer conditions of adjacent layers are the full-bonded condition at the normal temperature.

Case 2: the interlayer conditions of adjacent layers are the full-bonded condition at the high temperature.

Case 3: the interlayer conditions of adjacent layers are the ICB condition at the normal temperature.

Case 4: the interlayer conditions of adjacent layers are the ICB condition at the high temperature.

The axle load number and the rut depth will be predicted to reflect the performance of asphalt pavement. Firstly, assuming that the calculated deflection is equal to the designed deflection, the axle load number of the asphalt pavement within the design service life can be calculated according to the following equation [24,25]:

$$N_e = \left(\frac{600}{k \times l_d}\right)^5 \tag{10}$$

where N_e is the cumulative equivalent single axle loads number of a lane within design service life; k is a coefficient, and the recommended value for it is 1.0; l_d is the designed deflection (0.01 mm).

In order to get the deformation of the pavement structure, the accumulated rut depth (RD) in the entire asphalt pavement can be expressed in the following equation [26]:

$$\mathrm{RD} = \sum_{i=1}^{N} h^i \varepsilon_p^i \tag{11}$$

where RD means the permanent deformation of the asphalt pavement; N denotes the number of sublayers; h^i is the thickness of sublayer i; ε_p^i is the plastic strain in sublayer i. The strain ε_p^i in each of the pavement sublayers can be calculated by the vertical strain ε_z^i, and the relationship is as follows:

$$\frac{\varepsilon_p^i}{\varepsilon_z^i} = k_1 \times 10^{k_2} T^{1.5606} N_{cy}^{0.4791} \tag{12}$$

$$k_1 = (C_1 + C_2 \times dh) \times 0.328196^{dh} \tag{13}$$

$$C_1 = -0.1039 \times h_{ac}^2 + 2.4868 \times h_{ac} - 17.342 \tag{14}$$

$$C_2 = 0.0172 \times h_{ac}^2 - 1.7332 \times h_{ac} + 27.428 \tag{15}$$

where k_1 is the function of h_{ac} and dh; h_{ac} is the thickness of the total asphalt layers (in); dh is the depth from the surface (in); k_2 is calibration factor, and the recommended value for it is −3.79016; T

and N_{cy} are the temperature (°F) and the axle loads number respectively.

3. Response results and analysis

The responses of the pavement structure are computed by the different interlayer conditions and two kinds of temperature conditions, and these responses are applied to forecast the structural performance of asphalt pavement.

3.1 Structural responses with different interlayer condition

The structural responses are computed with the four cases mentioned before, and the results are listed in **Table 3**. The negative value denotes compressive response, and the positive value indicates tensile response. The responses of the three monitoring points with the full-bond condition are smaller than their responses with the ICB condition whether it is normal temperature or high temperature. Compared the responses in case 1 with the responses in case 3 (at the normal temperature), the U_{YA}, ε_{XB} and ε_{ZB} in case 1 are all a little greater than them in case 3, but the ε_{YC} in case 1 is obviously greater than it in case 3. Compared the responses in case 2 with the responses in case 4 (at the high temperature), the U_{YA} in case 2 is a little bigger than it in case 4, but the strain ε_{XB}, ε_{ZB} and ε_{YC} in case 2 are obviously bigger than them in case 4. Regardless of whether it is the normal temperature or the high temperature, the strain ε_{YC} at the top of the subgrade with the full-bond condition is significantly smaller than it is with the ICB condition. It may imply that the way of calculating the responses of asphalt pavement applying with the full-bond condition is possible to underrate the real responses of the asphalt pavement. In addition, the strain ε_{XB} and the strain ε_{YC} in case 2 are comparable with the results obtained by Xue Z. et al. [27], which indicate that the responses calculated by the ICB condition are basically reasonable and acceptable.

Table 3. Responses under different interlayer condition.

Case	U_{YA} (mm)	ε_{XB} (10^{-6})	ε_{ZB} (10^{-6})	ε_{YC} (10^{-6})
Case 1 ①	–0.1669	18.802	39.101	–82.186
Case 2 ②	–0.4894	40.310	55.016	–124.430
Case 3 ③	–0.1691	19.656	40.342	–101.056
Case 4 ④	–0.5068	87.771	106.547	–153.511
Ratio (((③ – ①)/①)*100%)	1.36%	4.55%	3.17%	22.96%
Ratio (((④ – ②)/②)*100%)	3.56%	117.74%	93.66%	23.37%

Assuming that the designed deflection equals the calculated deflection, then the cumulative numbers of the equivalent axle load at the normal temperature can be calculated by Equation (10), and the results are shown in **Figure 5(a)**. The cumulative numbers of the equivalent axle load in case 3 are smaller than those in case 1. It means that the ICB condition reaches the calculated deflection in advance compared with the full-bond condition. The predicted rut depth at the high temperature with one million of the equivalent axle load is shown in **Figure 5(b)**, and the rut depth in case 4 is greater than it in case 2. This denotes that the deformation of asphalt pavement with the ICB condition is more serious than it with the full-bond condition. Based on the above results, it's easy to know that by contrast with the structural responses under the ICB condition, the structural responses of the asphalt pavement with the full-bond condition are relatively small, or the real structure responses of the asphalt pavement are underestimated with the full-bond condition. It may be a good and proper cause to explain the reason for the early diseases of the asphalt pavement structure. Therefore, in the following sections, the ICB model will be applied to estimate the structural responses of the asphalt pavement with different conditions.

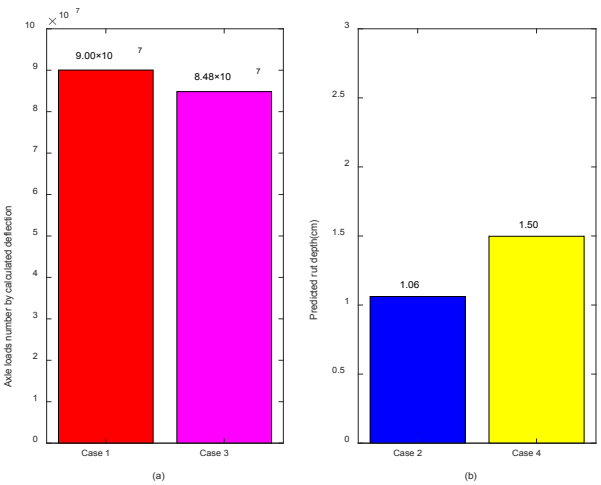

Figure 5. (a) Axle load numbers at the normal temperature and (b) rut depth of asphalt pavement at the high temperature.

3.2 Strains of the asphalt pavement structure under the ICB condition

The strain profile of the asphalt pavement structure is plotted by 56 points at the top of each structure layer, which ranges from 0 m to 0.55 m along the X-axis direction. Because the asphalt pavement structure is symmetrical about the Y axis, the structural responses of asphalt pavement on both sides can be plotted. **Figures 6(a) and (b)** present the strains of the asphalt pavement at the normal temperature, where ε_X is the transverse strain and ε_Z is the longitudinal strain. The longitudinal strains are in compression at the top of the surface course, and the transverse strains under the load position are also in compression. The transverse strains in other positions are very small and approach 0, and this reflects that the semi-rigid base has a strong supporting role in the asphalt concrete surface. The longitudinal strains are in tension at the bottom of the surface course, and the transverse strains under the load position are also in tension. The transverse strains in other positions are in compression. As shown in **Figure 6(b)**, the longitudinal strain ε_Z and transverse strain ε_X at the bottom of the semi-rigid base are all in tension, and the longitudinal strain ε_Z is less than the transverse strain ε_X at the same nodes. ε_Y is the vertical strain at the top of the subgrade, which is all negative, and this means that the subgrade is under pressure.

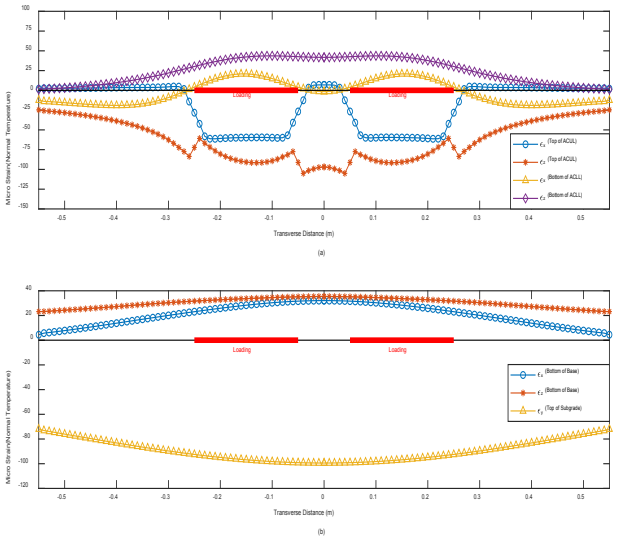

Figure 6. Strains of asphalt pavement at the normal temperature.

Figures 7(a) and (b) present the strains of the asphalt pavement at high temperatures. At the top of the surface course, the longitudinal strains are in compression, and the transverse strains under the loading position are also in compression. However, compared with the normal temperature, the transversely tensile strains at the top of the surface course change remarkably outside the edges of the dual tire, which are bigger than the transversely tensile strain at the bottom of the surface course. At the bottom of the surface course, the longitudinal strains are in tension, and the transverse strains under the loading position are also in tension, but the transverse strains in other positions are in compression. In **Figure 7(a)**, the transversely tensile strain at the top of the ACUL is greater than the strains at the bottom of the ACLL, which is similar to the trend obtained by Alae et al. [11], and the maximum of it reaches almost 460 micro strains.

From **Figures 6(b) and 7(b)**, the strains at normal and high temperatures have a similar trend. In **Figure 7(b)**, the transverse strains ε_X and the longitudinal strains ε_Z at the bottom of the semi-rigid base are almost in tension, and they are slightly larger than that at the normal temperature. The vertical strains ε_Y at the top of the subgrade are all in compression, which has an obvious increase compared with the

normal temperature. According to these results, it is easy to understand that the tensile strains at the top of the surface course with the high temperature may be the main reason for the top-down cracking, and this implies that the transversely tensile strains will be prone to cause the surface course to crack in the traffic direction (longitudinal direction) at the high temperature. This keeps consistent with the research results of Alae et al. [11], and is also basically the same as the conclusion of the classic model of top-down cracking.

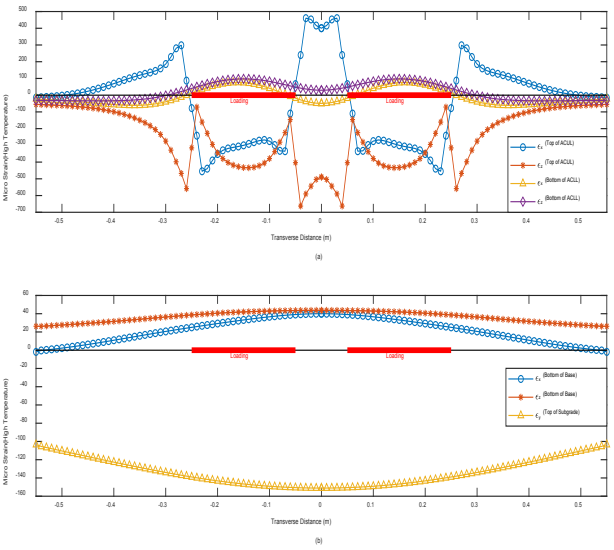

Figure 7. Strains of asphalt pavement at the high temperature.

3.3 Structural responses of asphalt pavement with local bond failure

For purpose of imitating the phenomenon of the local bond failure between two adjacent layers, two cases of bond failure are considered as follows:

Case 1: The local bond failure happens between the ACUL and ACML.

Case 2: The local bond failure happens between the ACLL and the semi-rigid base.

The disengaging area is used to denote the region of the local bond failure, and the five types of the disengaging area as shown in **Figure 4** are considered in this research. The responses of the three monitoring points as shown in **Figure 1** are computed when the different types of the disengaging area happened in Case 1 and Case 2. The results at the normal and high temperatures are listed in **Table 4** and **Table 5** respectively.

In **Table 4**, the responses have an obvious difference in Case 1 and Case 2, and they all keep rising when the disengaging area increases. From type "T0" to type "T4", the increment of the displacement U_{YA} in Case 1 is a little bigger than it is in Case 2, and the strain ε_{YC} has a slight increase in Case 1 and Case 2. However, the increment of the strain ε_{XB} in Case 2 is greater than it in Case 1, and the strain ε_{ZB} have the same trend as the strain ε_{XB}.

Although the responses in **Table 5** are larger than the responses in **Table 4** in the corresponding cases, they have a similar trend. From **Table 4** and **Table 5**, the variation of the displacement U_{YA} in case 1 is greater than that of the displacement U_{YA} in Case 2 at the normal temperature or the high temperature, which means that the influence of Case 1 on the displacement U_{YA} is relatively obvious compared with that of Case 2. The strain ε_{YC} has little change at the normal or high temperature, and this means the local bond failure has a little effect on it. But the strain ε_{XB} and the strain ε_{ZB} all increase observably in Case 1 and Case 2 as the size of disengaging area enlarges, especially in Case 2. It indicates the local bond failure between the bottom of the ACLL and the top of the semi-rigid base has a significantly negative impact on the tensile strains at the bottom of the ACLL, and this will be more serious with the high temperature. Hence, bottom-up cracking may be easy to form when the phenomenon of bond failure occurred between the ACLL and the semi-rigid base. In addition, compared with the interlayer bond failure between the ACUL and the ACML, it is easy to know that the influence of the local bond failure between the ACLL and the semi-rigid base on the strains at the bottom of the surface course is more obvious.

Table 4. Responses with bond failure at the normal temperature.

	Type	U_{YA} **(mm)**	ε_{XB} **(10^{-6})**	ε_{ZB} **(10^{-6})**	ε_{YC} **(10^{-6})**
Case 1	T0 ①	–0.1691	19.656	40.342	–101.056
	T1	–0.1692	19.668	40.360	–101.057
	T2	–0.1709	20.890	41.669	–101.074
	T3	–0.1723	22.852	44.312	–101.147
	T4 ②	–0.1727	23.049	45.198	–101.267
Ratio (((② – ①)/ ①)*100%)		2.13%	17.26%	12.04%	0.21%
Case 2	T0 ③	–0.1691	19.656	40.342	–101.056
	T1	–0.1691	19.952	41.055	–101.053
	T2	–0.1693	24.844	49.339	–101.090
	T3	–0.1697	27.151	54.195	–101.556
	T4 ④	–0.1706	29.219	58.047	–102.014
Ratio (((④ – ③)/ ③)*100%)		0.89%	48.65%	43.89%	0.95%

Table 5. Responses with bond failure at the high temperature.

	Type	U_{YA} (mm)	ε_{XB} **(10^{-6})**	ε_{ZB} **(10^{-6})**	ε_{YC} **(10^{-6})**
Case 1	T0 ①	–0.5068	87.771	106.547	–153.511
	T1	–0.5074	87.930	106.702	–153.511
	T2	–0.5308	97.610	116.280	–153.530
	T3	–0.5445	112.435	131.298	–153.652
	T4 ②	–0.5461	112.826	131.784	–153.838
Ratio (((2–1)/1)*100%)		7.75%	28.55%	23.69%	0.21%
Case 2	T0 ③	–0.5068	87.771	106.547	–153.511
	T1	–0.5068	92.260	115.710	–153.515
	T2	–0.5077	171.619	243.444	–153.580
	T3	–0.5112	202.647	307.269	–154.251
	T4 ④	–0.5158	223.442	351.672	–155.061
Ratio (((④ – ③)/ ③)*100%)		1.78%	154.57%	230.06%	1.01%

3.4 Structural responses of asphalt pavement under moving loads

To estimate the performance of the pavement structure with the moving loads, the structural responses of the three monitoring points as shown in **Figure 1** are computed with vehicle load passing through the surface of ACUL under different speeds. The path length of the moving loads is 720 cm in total, and the moving loads will go 9 cm forward in every iteration. When the moving loads along the traffic direction complete the load path, the iterative process ends. The responses of the three monitoring points are computed at the normal and high temperatures respectively, and the speed of the moving loads is assumed at 30 km/h, 60 km/h, 90 km/h and 120 km/h respectively.

The structural responses shown in **Figures 8(a)-**

(d) are under the condition of normal temperature, and the structural responses shown in **Figures 9(a)-(d)** are under the condition of high temperature. The extremums of the displacement U_{YA} decrease with the increase of vehicle speed whether it is the normal temperature or the high temperature. Furthermore, the value of the displacement under a moving load is basically consistent with Zhao Y. et al. [28] in amount and magnitude, which shows that the response with the ICB model under the moving load is credible. The strain ε_{XB} and the strain ε_{ZB} all have a course of compression, tension and compression, meanwhile, the maximum of the strain ε_{XB} and the strain ε_{ZB} all decrease with the vehicle speed increasing.

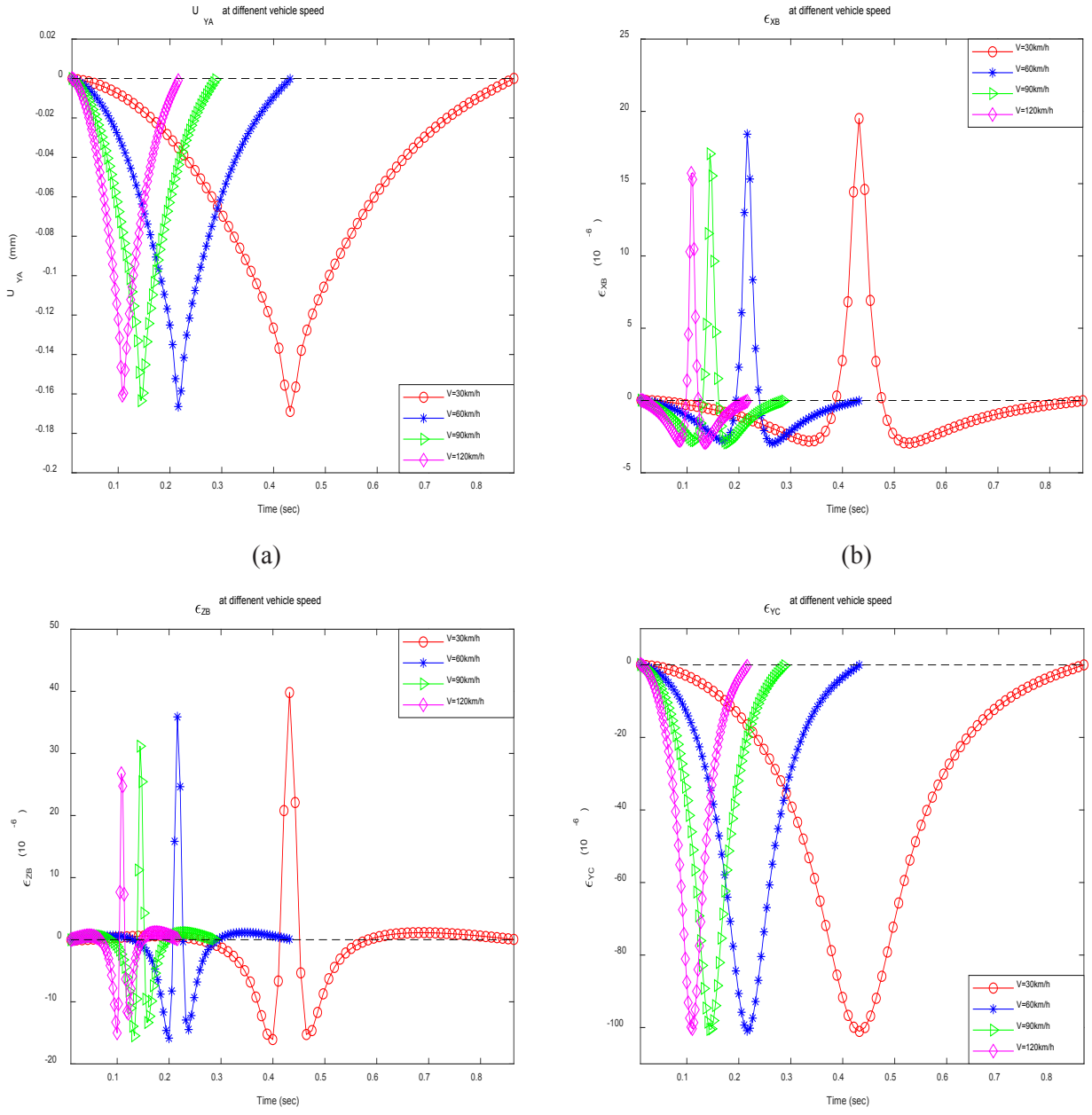

Figure 8. Response due to moving loads at the normal temperature.

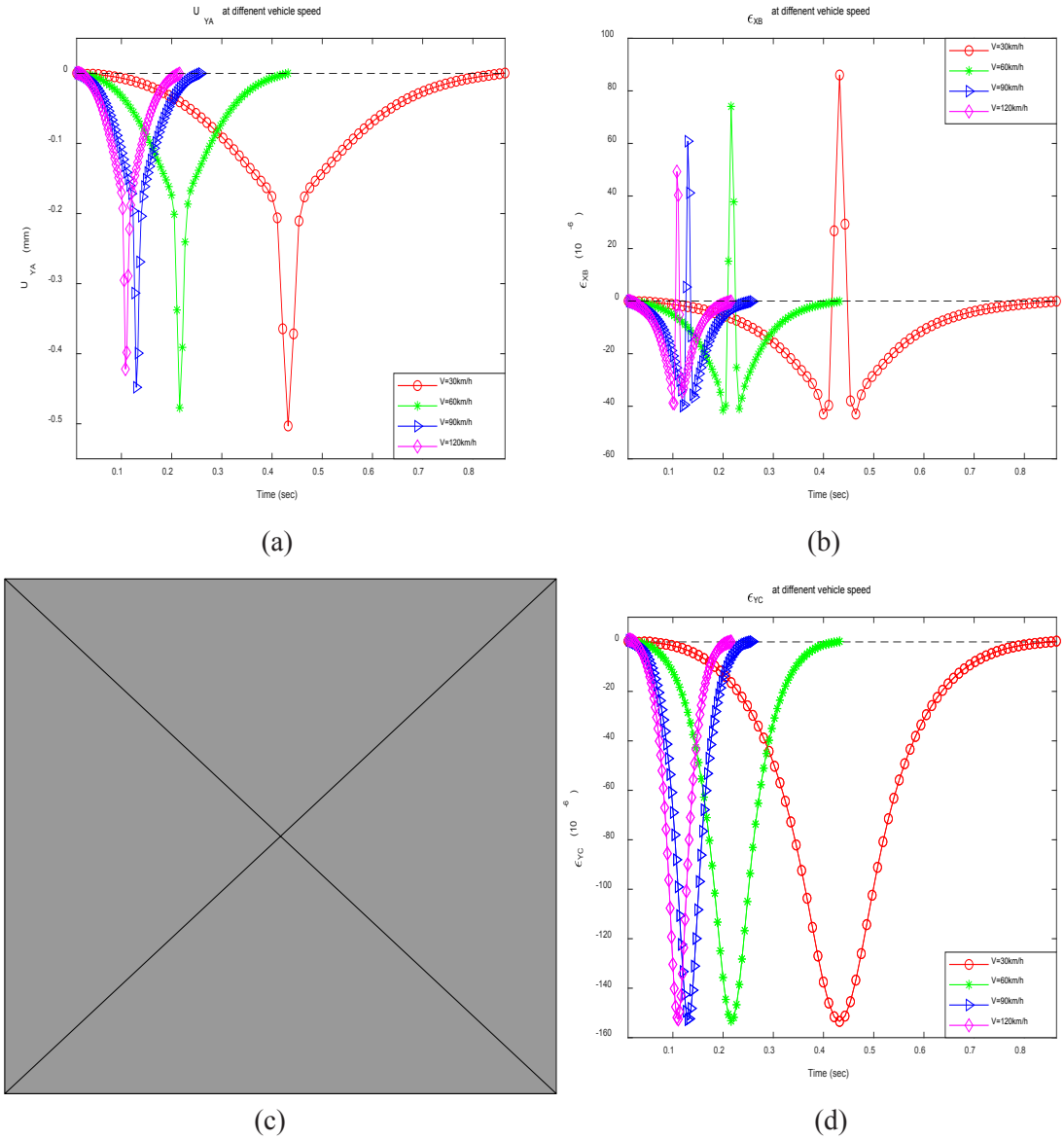

Figure 9. Response due to moving loads at the high temperature.

As vehicle speed increases from 30 km/h to 90 km/h at the normal temperature, the maximum of the strain ε_{XB} and the strain ε_{ZB} decrease by 12.46% and 21.70% respectively. As vehicle speed increases from 30 km/h to 90 km/h at a high temperature, the extreme the strain ε_{XB} and the strain ε_{ZB} decrease by 29.29% and 30.54% respectively. It may indicate that the deformation of asphalt pavement has a strong relationship with the loading time. The strain ε_{YC} under different speeds keeps almost same in the magnitude and trend at normal or high temperatures, and the extreme of the strain ε_{YC} is nearly the same under different speeds in **Figure 8(d)** or **Figure 9(d)**. It indicates that the vehicle load can be effectively transferred to the subgrade by the semi-rigid base. Furthermore, the structural responses of the surface course with the high temperature are significantly bigger than those with the normal temperature, which implies that the structural responses of asphalt pavement also have a strong relationship with the temperature of structural layers. In addition, the trends of structural responses at different vehicle speeds keep in correspondence with that obtained by Alae et al. [19]. So the material performance of asphalt concrete needs to be improved to resist the deformation at high temperatures.

4. Conclusions

The interlayer condition of structural layers of asphalt pavement not only has an effect on the absorption and dispersion of the external loads, but also is of great significance for accurately estimating the structural responses and performance of asphalt pavement. For simulating the interface condition of adjacent layers, the interlayer contact bonding model is applied to achieve the connection mode at the contact interface. To predict the structural behaviors of asphalt pavement with vehicle loads and consider the materials characteristics of asphalt pavement, the structural responses of asphalt pavement are computed with the interlayer contact bonding model at two different temperatures in this research. Furthermore, the structure responses to the local bond failure of the adjacent layer are also studied and the responses of pavement structure with the moving loads are also analyzed. Finally, some conclusions are presented as follows:

(1) Compared with the normal temperature the transversely tensile strains at the top of the surface course are easy to cause top-down cracking at the high temperature outside the edges of the dual tire. Because the influence range of vehicle loads is finite, a critical location for the formation of top-down cracking is the vicinity of the tire edge.

(2) The occurrence of the local bond failure between the ACLL and semi-rigid base breaks the integrality of the pavement structure and weakens the bonding strength between the ACLL and semi-rigid base, which makes the strains at the bottom of the ACLL increase with the increase of the disengaging area, especially at the high temperature. This may promote the chance of the initiation of the down-top cracking, hence, a strong bonding condition between the ACLL and the base needs to be constructed to restrain the occurrence of bond failure and resist the external loads together.

(3) The structural responses have a similar trend with the different vehicle speeds at normal or high temperatures. Although the extreme responses of the pavement structure decrease with the vehicle speed increasing, the asphalt pavement is still vulnerable to form deformation and damage at the interaction of lower speed and higher temperature. Therefore, it is necessary to reasonably limit the vehicle speed and further improve the material performance of asphalt concrete at high temperature.

Conflict of Interest

There is no conflict of interest.

Funding

This research was supported by the Scientific Research Program Funded by Shaanxi Provincial Education Department (Program No.21JK0830) and Shaanxi Provincial Natural Science Foundation Research Project (Program No.2022JM-166).

References

[1] Chun, S.Y., Kim, K., Greene, J., et al., 2015. Evaluation of interlayer bonding condition on structural response characteristics of asphalt pavement using finite element analysis and full-scale field tests. Construction and Building Materials. 96, 307-318.

[2] Kim, H., Arraigada, M., Raab, C., et al., 2011. Numerical and experimental analysis for the interlayer behavior of double-layered asphalt pavement specimens. Journal of Materials in Civil Engineering. 23(1), 12-20.

[3] Ozer, H., Al-Qadi, I.L., Wang, H., et al., 2012. Characterisation of interface bonding between hot-mix asphalt overlay and concrete pavements: Modelling and in-situ response to accelerated loading. The International Journal of Pavement Engineering. 13(2), 181-196.

[4] Zhang, Y., Wang, X., 2012. Impact of condition on mechanical response of asphalt pavement. Journal of Chang'an University (Natural Science Edition). 32(5), 7-11.

[5] Wu, S., Chen, H., Zhang, J., et al., 2017. Effects of interlayer bonding conditions between semi-rigid base layer and asphalt layer on mechanical responses of asphalt pavement structure.

International Journal of Pavement Research & Technology. 10(3), 274-281.

[6] Luo, Y., Zhang, Z., Zhang, K., 2018. Sensitivity analysis of influence factors on shear stress of asphalt pavement under high temperature. Engineering Journal of Wuhan University. 51(10), 895-900.

[7] Zhang, J., Wu, S., Pel J.Z., et al., 2014. Analysis of mechanical responses of asphalt pavement interlayers based on shear spring compliance. Journal of Highway and Transportation Research and Development (English Edition). 8(1), 1-6.

[8] Wellner, F., Hristov, B., 2015. Numerically supported experimental determination of the behavior of the interlayer bond in asphalt pavement. Transportation Research Record Journal of the Transportation Research Board. 2506, 116-125.

[9] Lazar, M.L., Diaconu, E., 2016. Influence of the interface conditions on flexible pavement structures life. Romanian Journal of Transport Infrastructure. 5(1), 30-37.

[10] Cao, D., Zhao, Y., Fu, G., 2017. Influence on the surface dynamic viscoelastic deflection of interlayer bonding condition. Journal of Beijing University of Technology. 43(4), 600-605.

[11] Alae, M., Zhao,Y., Zarei, S., et al., 2018. Effects of layer interface conditions on top-down fatigue cracking of asphalt pavements. International Journal of Pavement Engineering. 21(1), 1-9.

[12] Sun, L., Wang, G., Zhang, H., et al., 2018. Initiation and propagation of top-down cracking in asphalt pavement. Applied Sciences. 8(5), 1-14.

[13] Ashtiani, R.S., Morovatdar, A., Licon, C., et al., 2019. Characterization and quantification of traffic load spectra in texas overweight corridors and energy sector zones: Final report. Technical Report. doi: 10.13140 /RG.2.2.34611.78880.

[14] Morovatdar, A., Ashtiani, R., Licon, C., et al., 2019. Development of a mechanistic approach to quantify pavement damage using axle load spectra from south Texas overload corridors. Geo-Structural Aspects of Pavements, Railways, and Airfields (GAP 2019), Colorado Springs, CO, USA.

[15] Hu, X., Sun, L., 2005. Measuring tire ground pressure distribution of heavy vehicle. Journal of Tongji University(Natural Science). 33(11), 1443-1448.

[16] Dong, H., 2012. Asphalt pavement top-down cracks in laboratory test. Chang'an University, Xi'an, Shaanxi.

[17] Wang, X., Ma, X., 2020. Responses of semi-rigid base asphalt pavement with interlayer contact bonding model. Advances in Civil Engineering. (3), 1-13.

[18] Zhao, Y., Liu, H., Bai, L., et al., 2013. Characterization of linear viscoelastic behavior of asphalt concrete using complex modulus model. Journal of Materials in Civil Engineering. 25(10), 1543-1548.

[19] Alae, M., Zhao, Y., Leng, Z., 2020. Effects of ageing, temperature and frequency-dependent properties of asphalt concrete on top-down cracking. Road Materials and Pavement Design. (4), 1-21.

[20] Al-Qadi, I.L., Wei, X., Elseifi, M.A., 2008. Frequency determination from vehicular loading time pulse to predict appropriate complex modulus in mepdg. Asphalt Paving Technology: Association of Asphalt Paving Technologists-Proceedings of the Technical Sessions. 77, 739-771.

[21] Wang, X., Feng, J., Wang, H., et al., 2018. Effect of the dynamic load on stresses in a deck pavement with an interlayer contact model. Advances in Civil Engineering. (4), 1-10.

[22] Wang, X., Li, Y., Xu, H., 2011. ANSYS structural analysis unit and application. Beijing: China Communications Press.

[23] White, G., 2016. State of the art: Interface shear resistance of asphalt surface layers. International Journal of Pavement Engineering. 18(10), 887-901.

[24] JTG D50-2006, 2006. Specifications for design of highway asphalt pavement. Ministry of Transport of the People's Republic of China.

[25] Zhu, Y., Lei, M., Shi, N., et al., 2011. Influence

of interface condition on structural performance and life prediction of asphalt pavement. Highway Engineering. 36(5), 18-32.

[26] Siddharthan, R.V., Nasimifar, M., Tan, X., et al., 2016. Investigation of impact of wheel wander on pavement performance. Road Materials & Pavement Design. 1-18.

[27] Xue, Z., Wang, C., Zhang, W., et al., 2015. Research on pavement structure and material design of semi-rigid base long-life pavement. Journal of Highway and Transportation Research and Development. 32(10), 37-42,56.

[28] Zhao, Y., Liu, H., Bai, L., et al., 2012. Effect of constitutive relationship of asphalt mixture on pavement response. China Journal of Highway and Transport. 25(5), 6-11.